Electronic Supplementary Material (ESI) for ChemComm.

Supplementary Information

Benzothiadiazole-based covalent organic framework for highly efficient visible-light driven hydrogen evolution

Guang-Bo Wang,[†] Sha Li,[†] Cai-Xin Yan, Qian-Qian Lin, Fu-Cheng Zhu, Yan Geng[*] and Yu-Bin Dong[*]

College of Chemistry, Chemical Engineering and Materials Science, Collaborative Innovation Center of Functionalized Probes for Chemical Imaging in Universities of Shandong, Key Laboratory of Molecular and Nano Probes, Ministry of Education, Shandong Normal University, Jinan 250014, P. R. China.

[†] These authors contributed equally to this work.

Corresponding Authors: Y.-B. Dong, yubindong@sdnu.edu.cn
Y. Geng, gengyan@sdnu.edu.cn

1. Materials

All the commercially available chemicals were obtained from commercial suppliers and directly used without further purification. 4,4'-(benzothiadiazole-4,7-diyl)dibenzaldehyde was synthesized according to a slightly modified procedure published elsewhere.[1]

2. General instrumentation and methods

^{1}H spectrum of the monomer was recorded on a Bruker Avance 400 NMR spectrometer. Powder X-ray diffraction (PXRD) data were collected using a D8 ADVANCE X-ray with Cu Kα radiation (λ = 1.5405 Å). Fourier Transform Infrared (FT-IR) spectra in the region of 400-4000cm^{-1} were obtained with a Perkin-Elmer 1600 FT-IR spectrometer. Thermogravimetric analysis (TGA) was performed on a TA Instrument Q5 analyzer in the temperature range of 20-800 ^{o}C under an air atmosphere and a heating rate of 10 °C/min. Scanning electron microscopy (SEM) images of the COF materials were measured on a SUB010 scanning electron microscope with acceleration voltage of 20 kV and transmission electron microscopy (TEM) analysis was performed on a JEOL 2100 Electron Microscope at an operating voltage of 200 kV. X-ray photoelectron spectroscopy (XPS) data of **1** were obtained with a PHI 5000 Versaprobe II (VP-II) electron spectrometer from Ulvac-Phi using 300 W Al Kα radiation and the binding energies were referenced to the C1s line at 284.8 eV from adventitious carbon. Solid state ^{13}C CP-MAS NMR spectrum was acquired at 125.69 MHz using a 4 mm MAS NMR probe with a spinning rate of 8 kHz and a pulse width of 2.5 μs for a $\pi/4$ pulse, and 1800-2700 scans were accumulated with a 4 s recycle delay. UV-Vis spectra were recorded on a Cary 5000 UV-Vis spectrophotometer (Varian, USA). N_2 adsorption-desorption isotherm was obtained using an ASAP 2020/TriStar 3000 (Micromeritics) apparatus measured at 77 K, the sample was degassed at 100 ºC for 8h under high vacuum before analysis. Cyclic voltammetry (CV) measurements were performed on a CHI 660E in a three- electrode electrochemical cell equipped with a salt bridge and a scan rate of 100 mVs^{-1}. The auxiliary electrode was a platinum flakelet. The reference electrode was based on the Ag/Ag$^+$ couple. The working electrode was a glassy carbon electrode. Ferrocene/ferrocenium (Fc/Fc$^+$) redox potential was measured at the end of the experiment in order to calibrate the pseudo reference electrode as recommended by IUPAC. Generally, COF sample was dispersed in ethanol with a few droplets of Nafion solution and stirred for 3h. The suspension was then dropped on the glassy carbon electrode and dried to form thin films for measurements.

3. Synthesis procedures

Synthesis of 4,4'-(benzothiadiazole-4,7-diyl)dibenzaldehyde (BT)

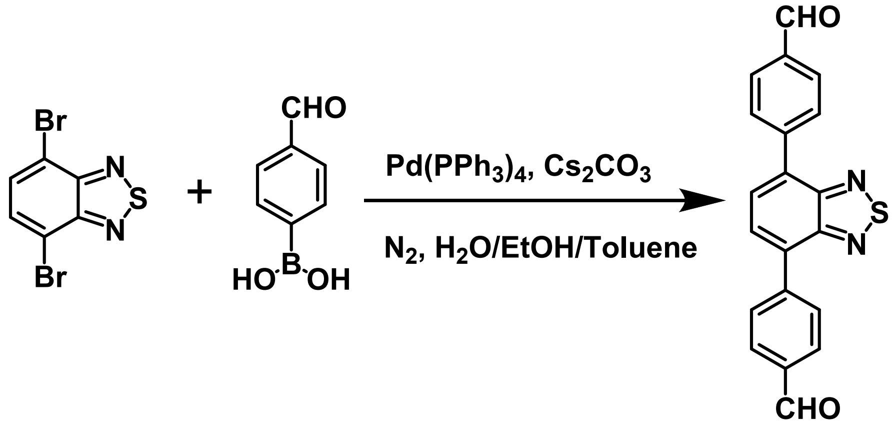

Generally, Cs_2CO_3 (25 mmol, 8.145 g), 4,7-dibromo-2,1,3-benzothiadiazole (5 mmol, 1.5 g) and 4-formylphenylboronic acid (12.5 mmol, 1.875 g) were introduced into a 100mL three-necked flask and degassed for three times. Then, H_2O, EtOH and toluene (1:2:3, v/v/v, 80 mL) and $Pd(PPh_3)_4$ (0.25 mmol, 0.290 g) were slowly added into the flask under N_2 atmosphere. After reflux for 48h under N_2, the mixture was poured into distilled water, extracted with chloroform, dried over $MgSO_4$ and evaporated under reduced pressure, giving the crude compound which was further purified by flash chromatography with dichloromethane as eluent to afford the title product as a yellowish green powder (743 mg, 72%). ^{1}H NMR (400 MHz, $CDCl_3$): δ 10.13 (s, 2H, CHO), 8.17-8.19 (d, 4H, Ph-H), 8.07-8.09 (d, 4H, Ph-H), 7.91 (s, 2H, Ph-H) ppm.

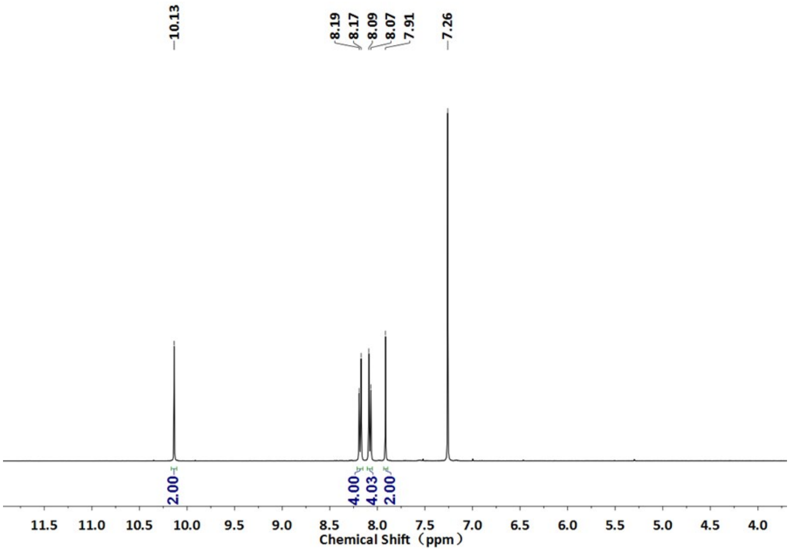

Fig. S1 ^{1}H NMR spectrum of 4,4'-(Benzothiadiazole-4,7-diyl)dibenzaldehyde (BT) in $CDCl_3$ (The peak at 7.26 ppm is related to the $CDCl_3$).

Synthesis of BT-TAPT-COFs (1)

A Pyrex tube was charged with 1,3,5-tris-(4aminophenyl)triazine (TAPT, 0.05 mmol, 17.7 mg) , 4,4'-(benzothiadiazole-4,7-diyl)dibenzaldehyde (BT, 0.075 mmol, 25.8 mg), 1,2-dichlorobenzne (1 mL) and n-butanol (1 mL), the mixture was sonicated for 5 minutes and an yellowish green suspension solution was obtained. Subsequently, 0.2 mL aqueous acetic acid (3 M) was added and this mixture was homogenized by sonication for another 5 minutes. Afterwards, the tube was flash frozen at 77 K (liquid N_2 bath) and degassed by three-freeze-pump-thaw cycles for three times, sealed under vacuum and then heated at 120 ºC for 3 days. After cooling down to room temperature, the yellow precipitate was collected by centrifugation and washed with N,N-dimethylformamide, THF and acetone, respectively. The resulting solid was Soxhlet extracted in THF and dried under vacuum at 100 ºC to afford the yellow powders of **1**.

4. Details of the Photocatalysis experiments

Photocatalytic H_2 evolution experiment

For a typical H_2 evolution experiment, a Pyrex tube was charged with the activated COF powder (2 mg), 0.1 M ascorbic acid water solution (10 mL) and hexachloroplatinic acid (10μL, 8wt% aqueous solution) as a platinum precursor. The pH value of the mixed solution was adjusted to 5 with HCl and NaOH aqueous solution. After deoxygenation with argon for 30 min, CH_4 gas is injected into the tube as an internal standard to quantify the amount of photogenerated H_2 gas. The system was connected to the device and irradiated with a 300 W Xenon lamp equipped with an UV cut-off filter ($\lambda \geq 420$ nm) under constant agitation and fan cooling for real time quantitative hydrogen detection. The generated H_2 was quantitatively measured by drainage gas-collecting method using a gas-tight syringe and analyzed by GC analysis (TianMei-7890Ⅱ) equipped with a molecular sieve column (5 Å) and a thermal conductivity detector (TCD) with argon as the carrier gas. For every series of the H_2 evolution experiment, two independent measurements were repeated for reproducibility. After the photocatalysis experiment, the COF material was recovered by washing with water and acetone then dried under vacuum at 100 ºC for multiple runs.

External quantum efficiency (EQE) measurement

In the EQE measurement, the accurate illumination power for a certain place (1 cm^2) was measured using a digital photodiode power meter (Newport, model 842-PE). The photocatalytic H_2 evolution was carried out in a special-made spectro-cell with a total volume of 7 mL and a path-length of 1 cm. The cuvette was filled with COF powder (0.1 mg), 2.0 mL solution of $H_2PtCl_6{\bullet}6H_2O$ (0.015 mg) and ascorbic acid under pH value of 5. After sealing and deoxygenation with argon for 15 min, CH_4 was add into the spectro-cell as an internal standard. Under constant stirring, the solution was irradiated by LED lamps (410 and 450 nm) at the same place and area (1 cm^2), where the light intensity was measured. The number of absorbed photons was calculated from the illumination power and absorbance of the reaction solution and the number of generated H_2 was obtained by GC. The external quantum efficiencies were estimated using the following equation:

$$\eta_{EQE} = 2 \times \frac{\text{Numbers of evolved hydrogen molecules}}{\textit{Numbers}\ \text{of the incident protons}} \times 100\%$$

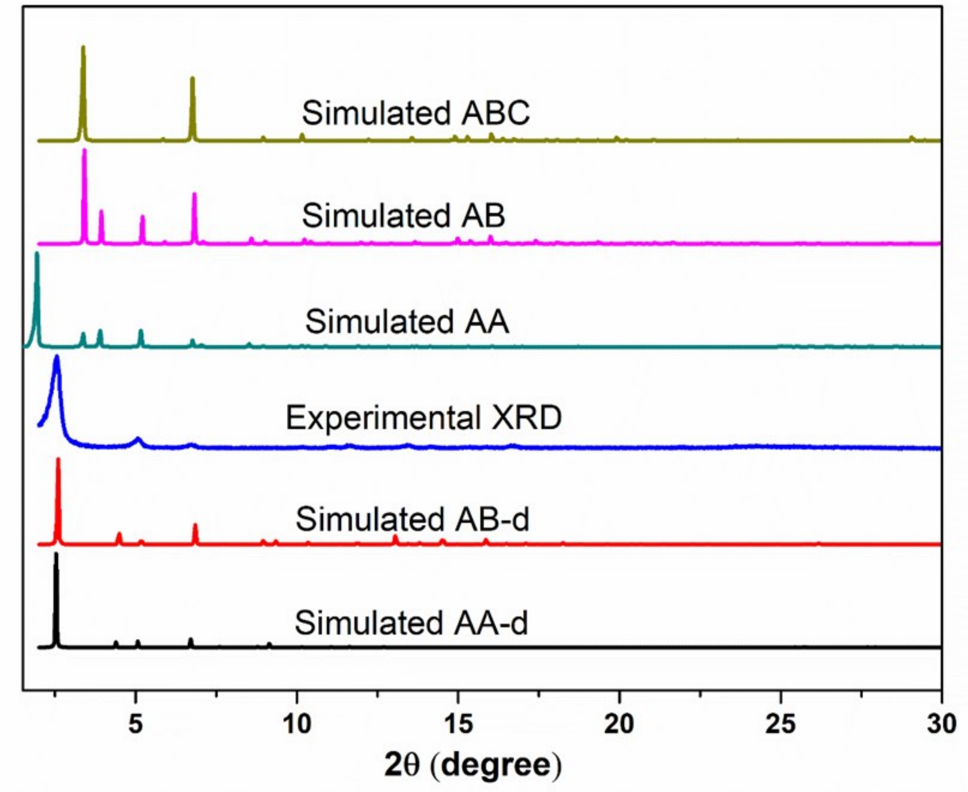

Fig.S2 Comparison of the experimental PXRD pattern of **1** with the simulated possible stacking models, where the AA, AB, ABC stackings are related to the formation of regular hexagonal pores, while AA-d and AB-d stacking models represent some distortions of the hexagonal pores of **1**.

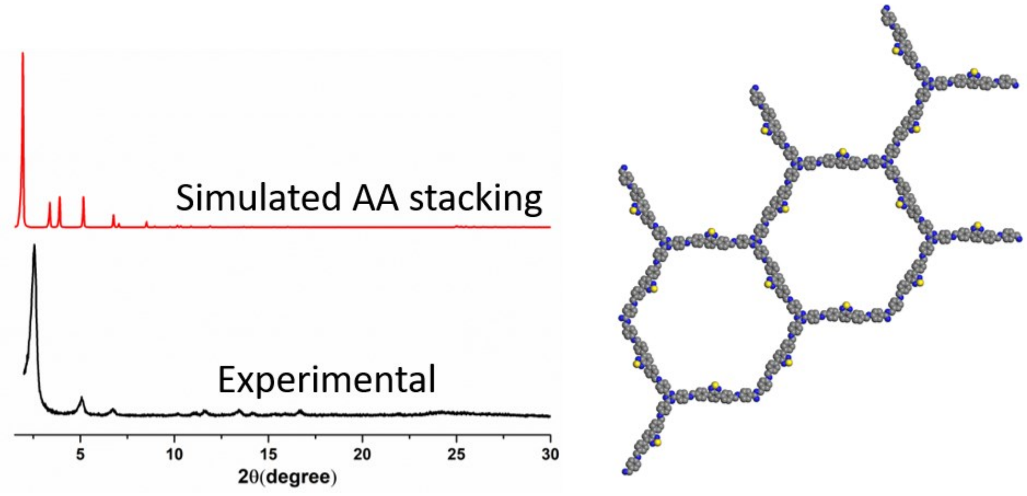

Fig. S3 Comparison of the experimental (black) and simulated AA stacking PXRD patterns of **1** and the top view of the simulated structure of AA stacking.

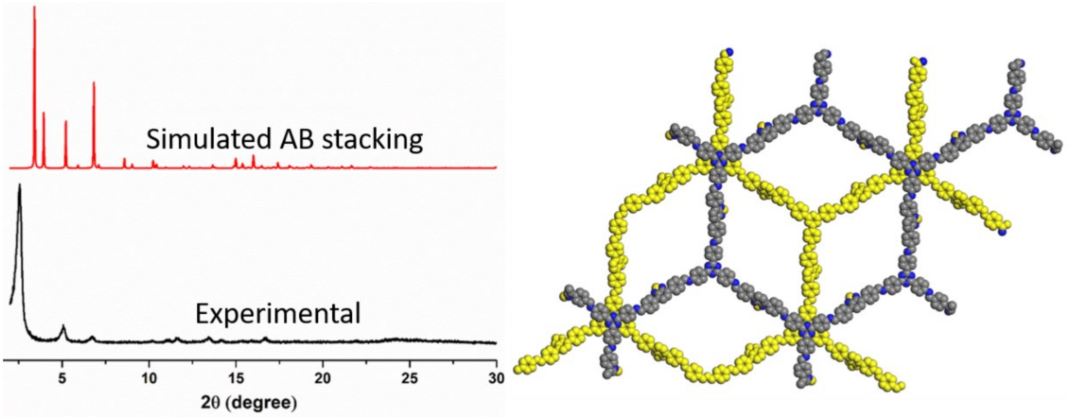

Fig. S4 Comparison of the experimental (black) and simulated AB stacking PXRD patterns of **1** and the top view of the simulated structure of AB stacking.

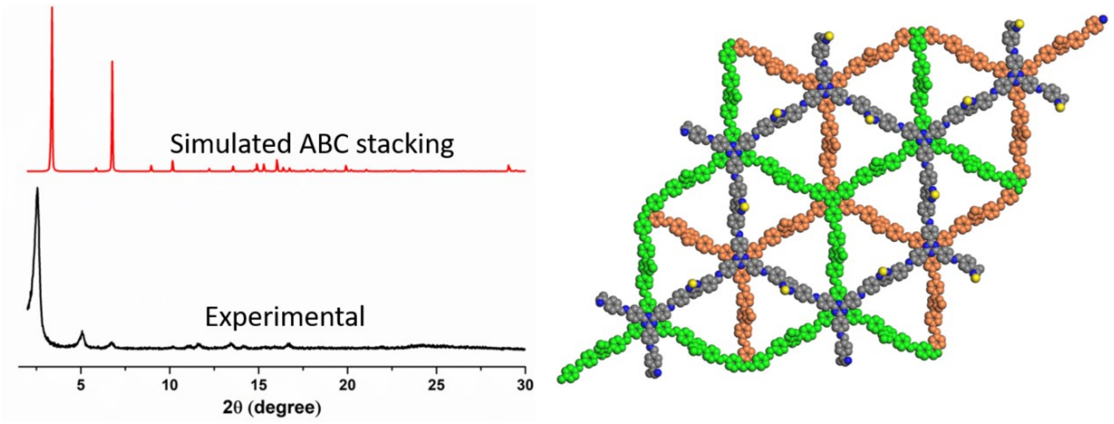

Fig. S5 Comparison of the experimental (black) and simulated ABC stacking PXRD patterns of **1** and the top view of the simulated structure of ABC stacking.

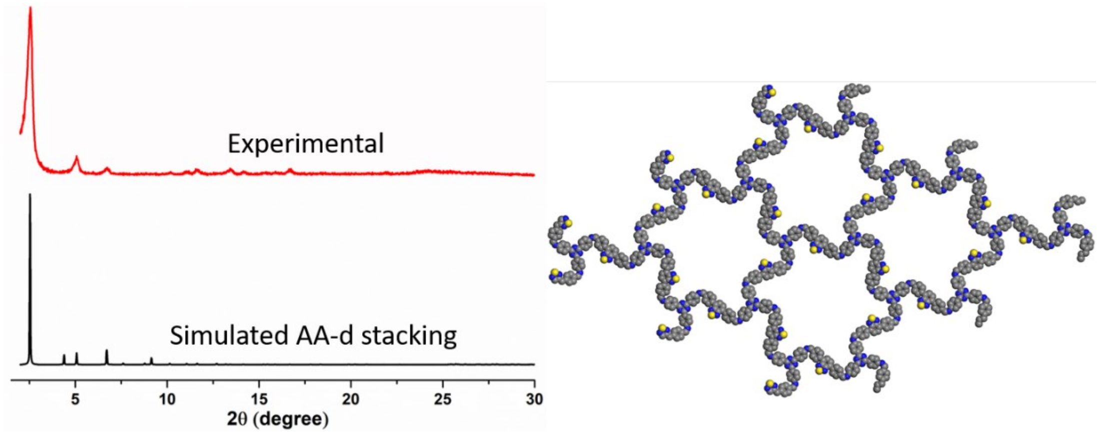

Fig. S6 Comparison of the experimental (black) and simulated AA-d stacking PXRD patterns of **1** and the top view of the simulated structure of AA-d stacking.

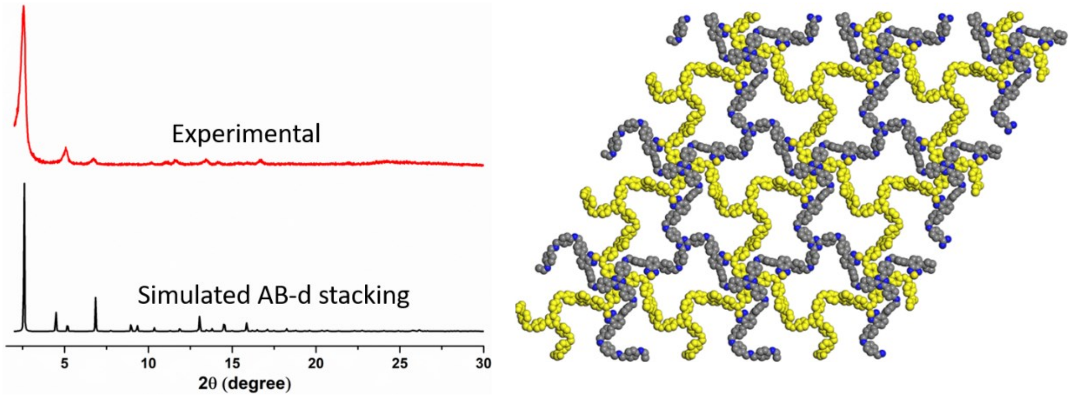

Fig. S7 Comparison of the experimental (black) and simulated AB-d stacking PXRD patterns of **1** and the top view of the simulated structure of AB-d stacking.

Table S1. Atomistic coordinates for the AA stacking mode of **1** optimized using Forcite method.

Space group: P3 (143) a = b = 39.6816 Å, c = 3.5379 Å $\alpha = \beta = 90.0°$, $\gamma = 120.0°$			
Pawley refinement	R_{wp}=4.34%, R_p=3.15%		
C1	0.37114	0.67317	0.89647
C2	0.41766	0.65108	0.7224
C3	0.45479	0.6555	0.74041
C4	0.48486	0.68789	0.92299
C5	0.47836	0.71742	1.05447
C6	0.44164	0.7137	1.03052
C7	0.41078	0.67973	0.87882
C8	0.54052	0.67324	0.93668
N9	0.523	0.6934	0.98494
C10	0.48919	0.60098	0.93787
C11	0.47938	0.56259	0.85783
C12	0.5058	0.5547	0.66708
C13	0.54085	0.58599	0.53689
C14	0.5501	0.62408	0.61289
C15	0.52444	0.63239	0.80905
C16	0.52457	0.50265	0.63093
C17	0.51509	0.46479	0.57825
C18	0.47761	0.43572	0.4547
C19	0.44944	0.44723	0.4161
C20	0.45867	0.48543	0.49587
C21	0.49655	0.51411	0.59801
C22	0.42988	0.36353	0.33612
C23	0.4224	0.32633	0.22864

C24	0.45301	0.31899	0.15368
C25	0.49089	0.35077	0.17552
C26	0.49812	0.38802	0.24383
C27	0.46832	0.39534	0.34585
N28	0.46436	0.26224	0.02774
C29	0.44239	0.2781	0.05512
C30	0.51772	0.25128	0.1993
C31	0.55754	0.26362	0.22718
C32	0.58508	0.30071	0.08816
C33	0.57204	0.32274	-0.10916
C34	0.53236	0.30831	-0.16011
C35	0.50525	0.27514	0.03108
C36	0.6273	0.31737	0.1425
N37	0.56224	0.526	0.72301
S38	0.58673	0.50136	0.74691
N39	0.54563	0.45966	0.63788
N40	0.29526	0.65888	0.90685
N41	0.65084	0.35674	0.13833
H42	0.39446	0.6259	0.57801
H43	0.45996	0.63462	0.60051
H44	0.50179	0.74238	1.19306
H45	0.4366	0.73595	1.14872
H46	0.57154	0.68837	0.99419
H47	0.47013	0.60566	1.11843
H48	0.45211	0.53903	0.96395
H49	0.56082	0.58102	0.36819
H50	0.57773	0.64743	0.51378
H51	0.42046	0.42779	0.30718
H52	0.43607	0.49289	0.46321

H53	0.40539	0.36686	0.41423
H54	0.39235	0.30296	0.21566
H55	0.51648	0.34915	0.15516
H56	0.52805	0.41069	0.21912
H57	0.41147	0.25787	0.02424
H58	0.49633	0.2242	0.32632
H59	0.56668	0.24567	0.37925
H60	0.59294	0.34998	-0.24099
H61	0.5224	0.32336	-0.33929

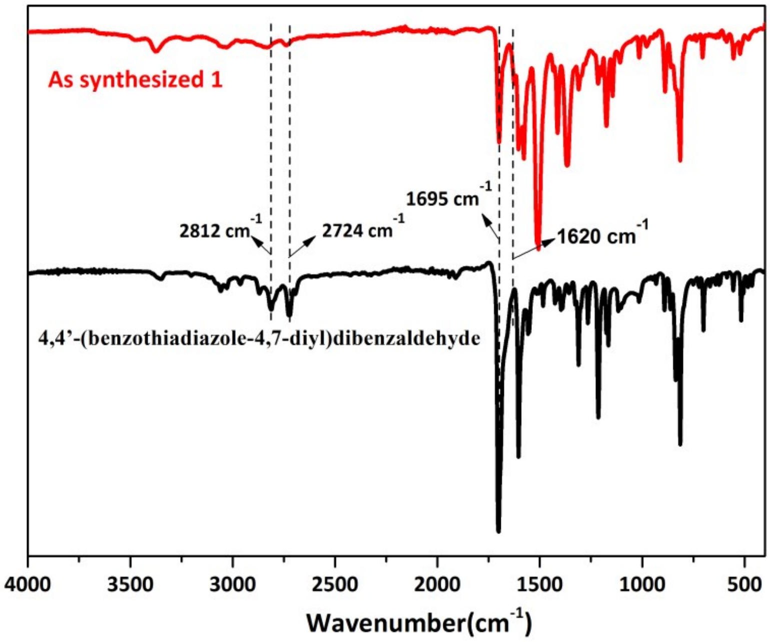

Fig. S8 Comparison of the FT-IR spectra of **1** and the BT monomer.

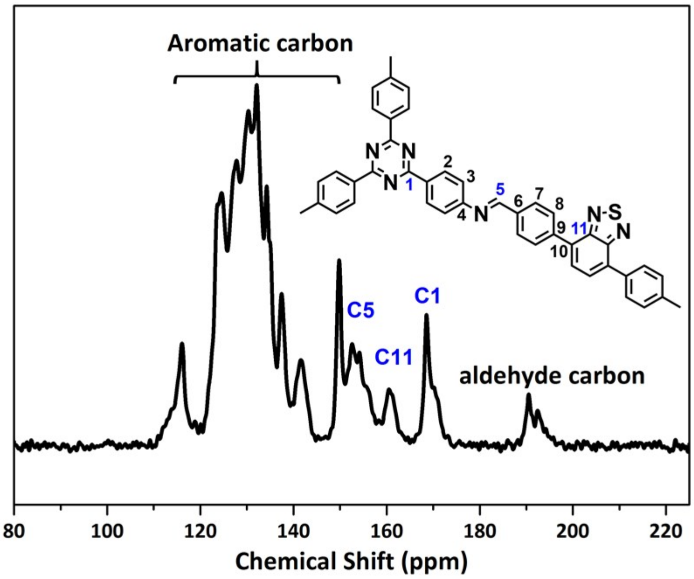

Fig. S9 The solid state ^{13}C cross polarization magic angle spinning (^{13}C CP/MAS) NMR spectrum of **1.**

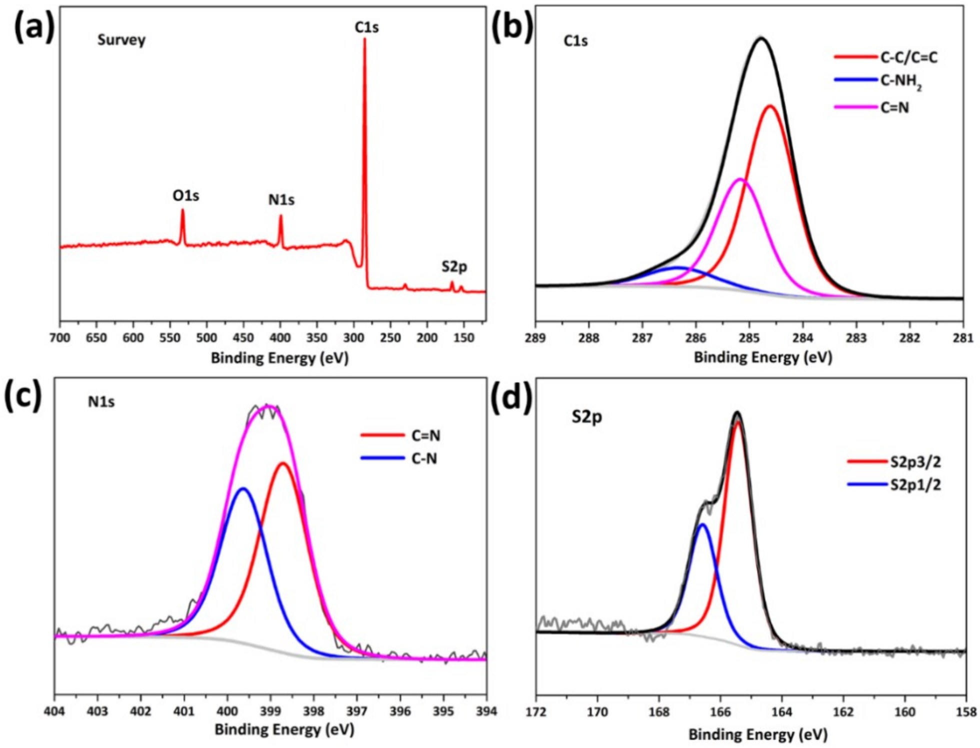

Fig. S10 (a) Survey, (b) C1s, (c) N1s and (d) S2p spectra of **1**. The C1s spectrum can be deconvoluted into three peaks with binding energies at 284.6, 285.2 and 286.2 eV, which are assigned to the aromatic sp^2 carbon, C-NH$_2$ and triazine carbon, respectively.

In the N1s spectrum, the peaks at 398.8 and 399.8 eV are attributed to the C=N and C-N, respectively. S2p spectrum shows a doublet characteristic (at 165.5 and 166.5 eV) to sulfur in the benzothiadiazole units.

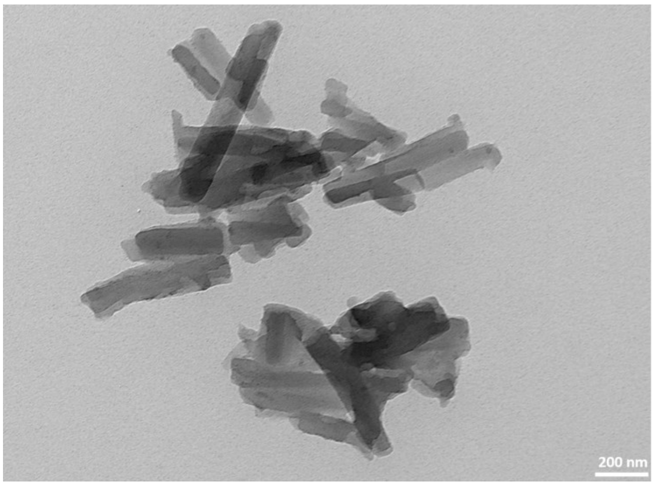

Fig. S11 Transmission electron microscopy (TEM) image of **1**.

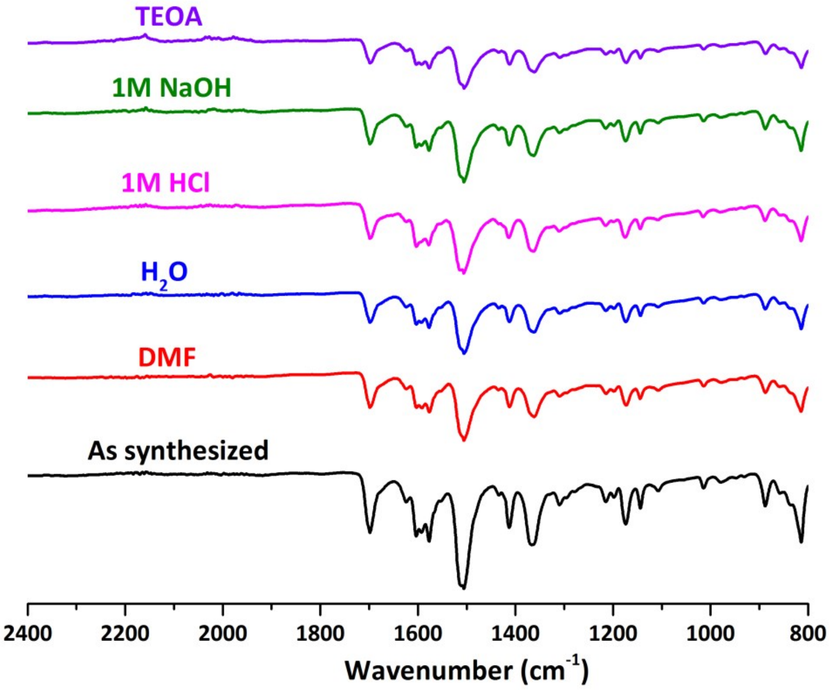

Fig. S12 FT-IR spectra of **1** after immersed in different solvents for 7 days.

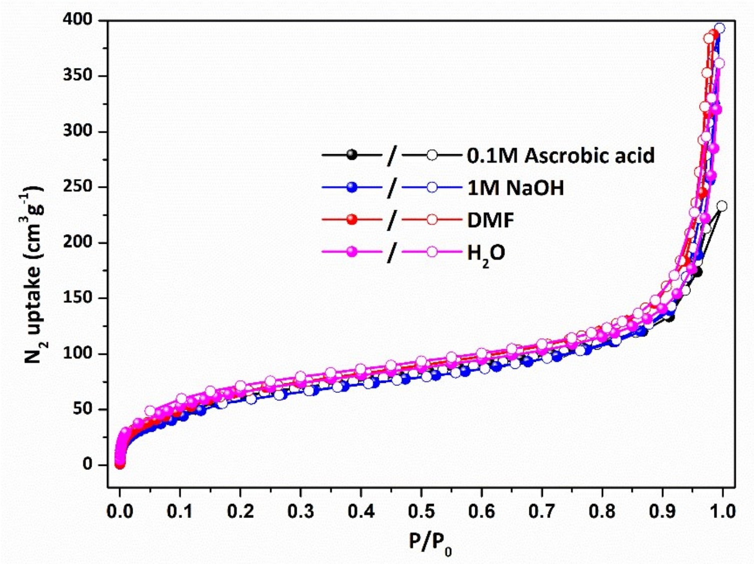

Fig.S13 N_2 adsorption isotherms of the samples that immersed in different solvents for 1 week.

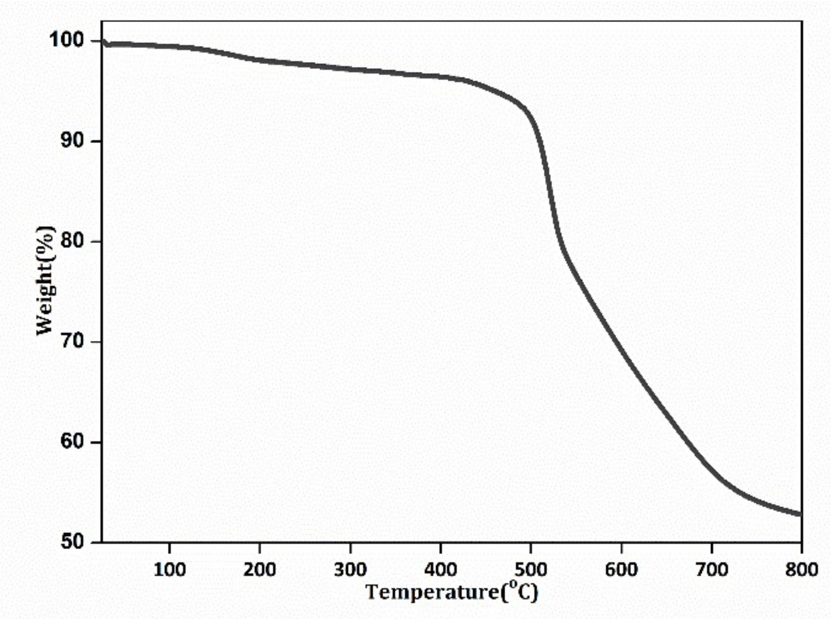

Fig. S14 TGA curve of **1** measured at a heating rate of 10 ºC/min under an air flow.

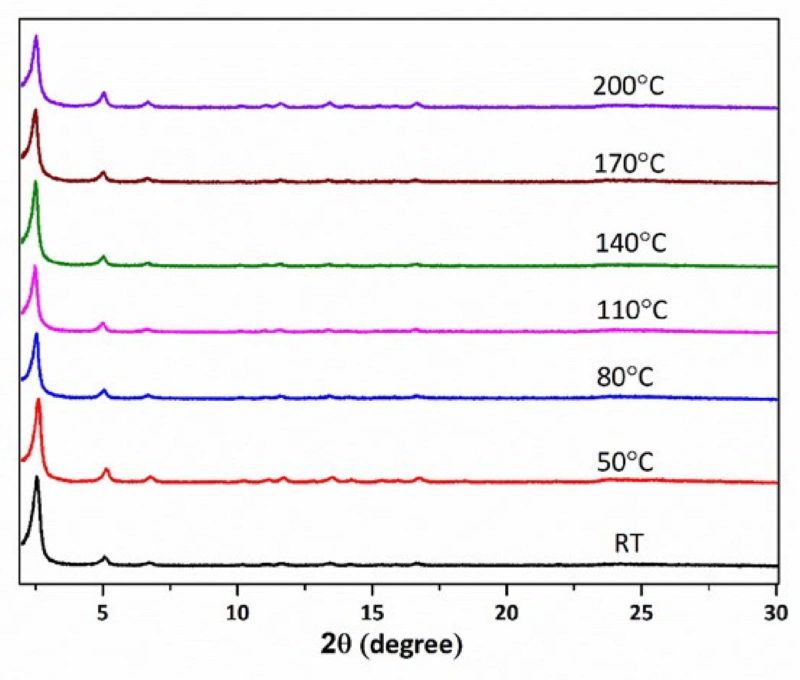

Fig. S15 Temperature-programming PXRD patterns of **1** up to 200˚C with the temperature interval of 30˚C.

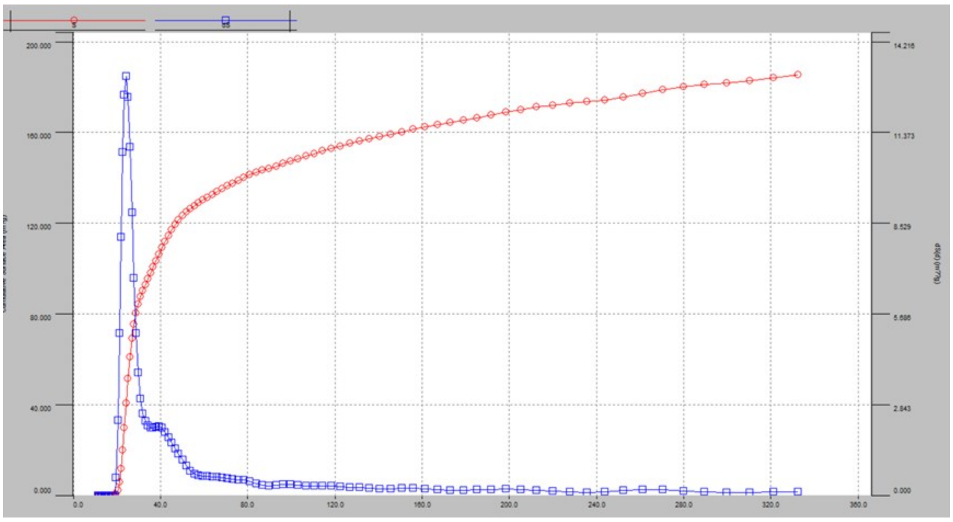

Fig. S16 Pore size distribution of BT-TAPT-COF (~24 Å) calculated from N_2 adsorption-desorption data using the QSDFT with the fitting error of 1.945%.

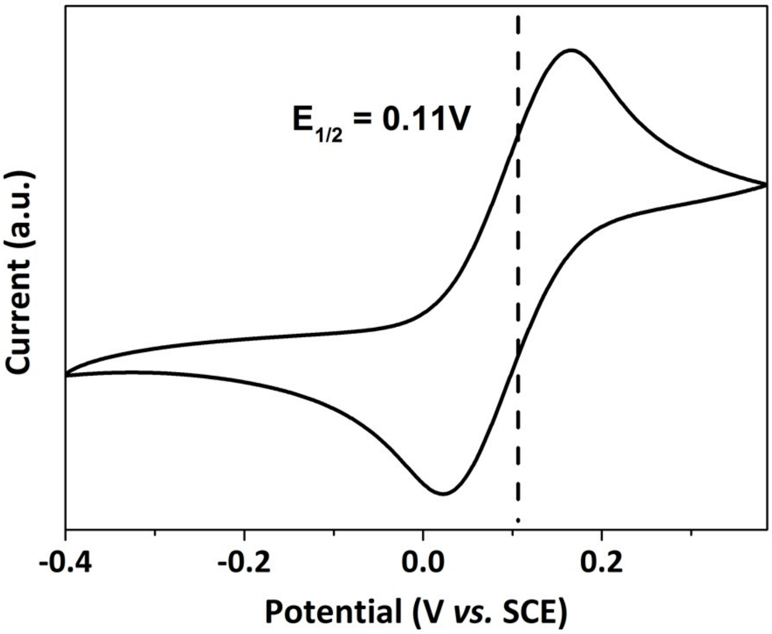

Fig. S17 Cyclic voltammetry measurements of ferrocene/ferrocenium couple to calibrate the pseudo reference electrode.

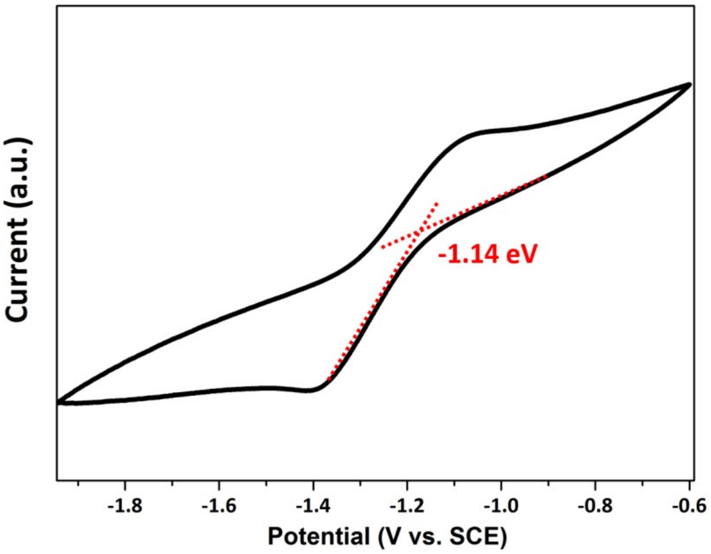

Fig. S18 Cyclic voltammetry plot of **1** referenced to saturated calomel (SCE) using ferrocene (Fc) as an internal standard at a scan rate of 100 mV S^{-1}.

The calculation of the E_{HOMO} and E_{LUMO} is according to the following equations[2]:

$$E_{LUMO} = -\left(E_{onset\ vs.\ SCE} - E_{1/2,Fc} + 4.8\right)eV$$

$$E_{HOMO} = E_{LUMO} - E_{g,opt}$$

Where, $E_{1/2,\ Fc}$ is obtained to be 0.11 vs. SCE., reduction onset potential ($E_{onset\ vs.\ SCE}$) was extracted from the x-intercept of the linear fit in the voltammogram, $E_{g,opt}$ is obtained from the UV-Vis spectrum by using Tauc plot method.

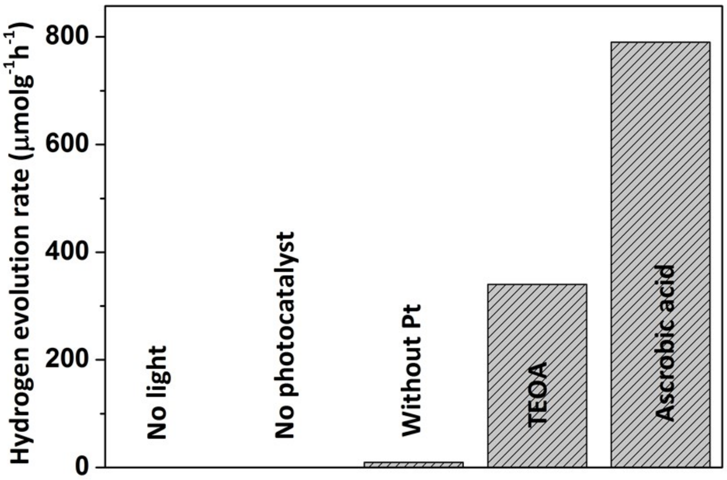

Fig. S19 Photocatalytic performance of **1** over 5h under visible-light irradiation in the absence of light/ photocatalyst/Pt co-catalyst and in the presence of sacrificial agent of TEOA/ascorbic acid.

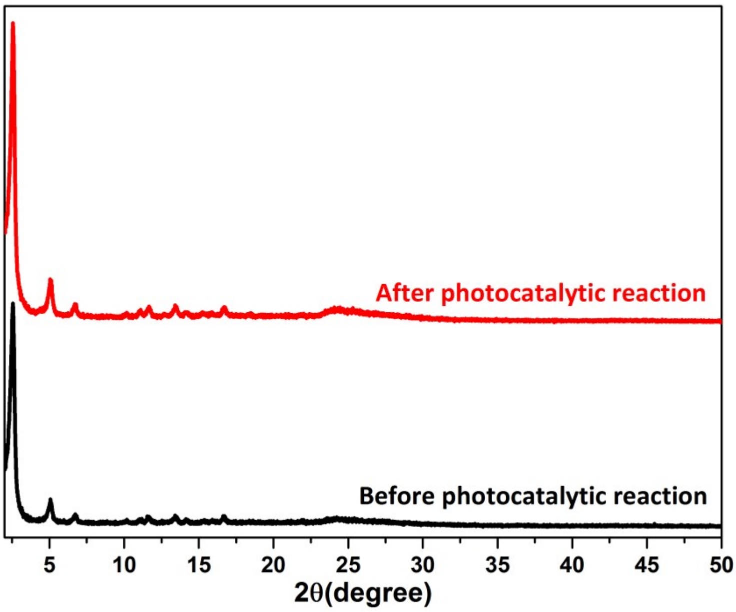

Fig. S20 PXRD patterns of **1** before and after photocatalytic hydrogen evolution reactions.

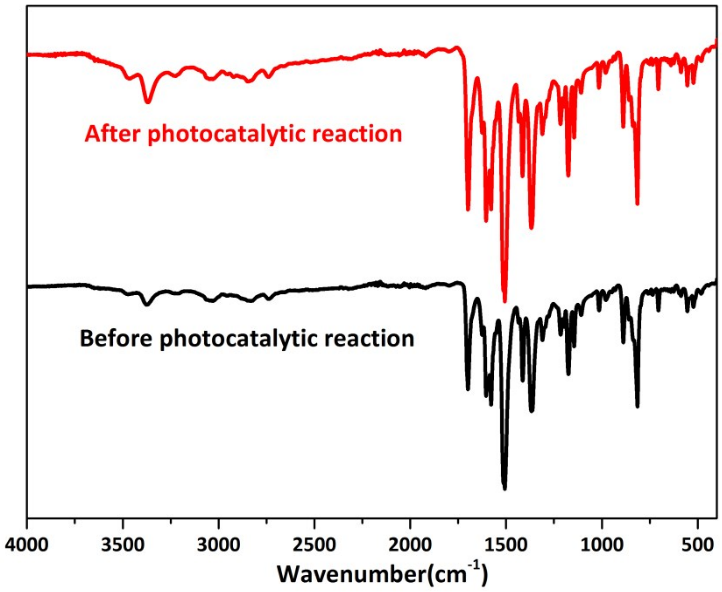

Fig. S21 FT-IR spectra of **1** before and after photocatalytic hydrogen evolution reactions.

Table S2. The summary of the photocatalytic H_2 evolution performance under visible-light irradiation over different types of CMPs and COFs.

COFs	**Band gap (eV)**	**Co-catalyst**	**Sacrificial agent**	**HER (μmolg^{-1}h^{-1})**	**AQY (%)**	**Ref.**
g-$C_{40}N_3$-COF	2.36	Pt	Na_2S	4	-	3
g-$C_{40}N_3$-COF	2.36	Pt	TEA	12	-	3
g-$C_{40}N_3$-COF	2.36	Pt	Na_2SO_3	14	-	3
N_0-COF	2.6-2.7	Pt	TEOA	23	0.0017 (500 nm)[c]	4
TpPa-2-COF	2.52	Pt	Lactic acid	28	-	5
g-$C_{40}N_3$-COF	2.36	Pt	EtOH	56	-	3
TpPa-2	2.07	Pt	Sodium ascorbate	72.09	-	6
BE-COF	2.12	Pt	Ascorbic acid	76.0	-	7
PTP-COF	2.1	Pt	TEOA	83.83	-	8
N_1-COF	2.6-2.7	Pt	TEOA	90	0.077 (450 nm)[c]	4
N_1-COF	-	Co-1	TEOA	100	-	9
CTP-1	2.96	Pt	TEOA	120	-	10
sp^2 c-CMP	1.96	Pt	TEOA	140	-	11
TTR-COF	2.71	Au	TEOA	141	-	12

TTB-COF	2.8	Au	TEOA	145.25	-	12
N3-COF	-	Co-1	TEOA	163	-	9
OB-POP-1	2.21	Pt	TEOA	168	-	13
CTF-1	2.23	Pt	TEOA	168	-	14
B-CTF-1	2.14	Pt	TEOA	179	-	14
TpPa-COF-NO_2	1.92	Pt	Sodium ascorbate	220	-	15
COF-42	-	Co-1	TEOA	233	-	9
TP-BDDA	2.31	Pt	TEOA	324 ± 10	1.8 (520 nm)[d]	16
CTF-15	2.58	Pt	TEA	352	15.9 (420 nm)[e]	17
TBC-COF	-	Pt	TEOA	360	0.87 (420 nm)[d]	14
N_2-COF	-	Co-2[b]	TEOA	414	-	9
N_2-COF	2.6-2.7	Pt	TEOA	438	0.19 (450 nm)[c]	4
CTP_{300}	2.36	Pt	TEOA	500	2.4 (405 nm)	10
N_2-COF	-	Co-1[a]	TEOA	782	0.16[d]	9
OB-POP-2	2.28	Pt	TEOA	940	-	13
TpDTz COF	2.07	NiME	TEOA	941	0.2 (400 nm)[d]	18
CTF-1-10min	2.26	Pt	TEOA	1072	9.2 (450 nm)[d]	19
CTF-Th	2.38	Pt	TEOA	1100	-	20
OB-POP-4	2.37	Pt	TEOA	1114	-	13
TpPa-1-COF	2.02	Pt	Sodium ascorbate	1223	-	21
OB-POP-3	2.14	Pt	TEOA	1322	2.0 (420 nm)	13
sp^2 c-COF	1.9	Pt	TEOA	1360	-	11
CTF-O	2.67	Pt	TEOA	1440	2.10 (420 nm)	22
CTF-HUST-1	2.03	Pt	TEOA	1540	-	23
TpPa-COF	2.09	Pt	Sodium ascorbate	1560	-	15
TP-COF	2.28	Pt	Ascorbic acid	1600 (±80)	-	24
N_3-COF	2.6-2.7	Pt	TEOA	1703	0.44 (450 nm)[c]	4
CTF-BT	2.51	Pt	TEOA	1800	-	20
$Ni(OH)_2$-2.5%/TpPa-2	-	$Ni(OH)_2$	Sodium ascorbate	1895.99	-	6
TFPT-COF	2.8	Pt	TEOA	1970	2.2 (400 nm)[f]	25
$CTFS_{10}$	1.87	Pt	TEOA	2000	-	26
sp^2 c-COF_{ERDN}	1.85	Pt	TEOA	2120	0.48 (495 nm)	11
COF-alkene	2.34	Pt	TEOA	2330	6.7% (420nm)[d]	27
g-$C_{40}N_3$-COF	2.36	Pt	TEOA	2596	4.84(±0.27) (420 nm)	3
TpPa-COF-CH_3	2.10	Pt	Sodium ascorbate	3070	-	15
CdS-COF(90:10)	-	Pt	Lactic acid	3678	4.2 (420 nm)	5
TZ-COF-4	2.2	Pt	Ascorbic acid	4296	1.3% (420nm)[e]	28

S-COF	2.10	Pt	Ascorbic acid	4440 (±140)	-	24
PyTA-BC	2.71	Pt	Ascorbic acid	5030	1.46 (420nm)	29
CTF-S	2.47	Pt	TEOA	5320	4.11 (420 nm)	22
TpPa-1	2.11	Pt	Ascorbic acid	5479	-	30
MoS2-3%/TpPa-1-COF	2.14	MoS_2	Ascorbic acid	5585	0.76 (420 nm)^d	30
CTF-$HS_{0.75}$-1	2.70	Pt	TEOA	6040	4.2 (420 nm)	23
CTF-BT/Th-1	2.51	Pt	TEOA	6606	7.3(420 nm)^d	20
CTF-$HS_{0.75}$-2	-	Pt	TEOA	7100	6.8 (420 nm)	23
TpPa-COF-$(CH_3)_2$	2.06	Pt	Sodium ascorbate	8330	-	15
TP-COF	1.97	PVP-Pt	Ascorbic acid	8420	0.4 (475 nm)^d	7
CTF-CBZ	2.17	Pt	TEOA	9920	4.07 (420 nm)	31
CN-COF	2.09	Pt	TEOA	10100	20.7 (425 nm)^d	32
Pd^0/TpPa-1-EosinY	-	-	TEOA	10400	-	33
CTF-N	2.17	Pt	TEOA	10760	4.07 (420 nm)	31
20%CdS-CTF-1	-	Pt	Lactic acid	11430	16.3 (420 nm)	34
CdS NPs/3%CTF-1	2.36	Pt	Lactic acid	12150	-	35
Mo_3S_{13}@EB-COF	-	$Ru(bpy)_3Cl_2$	Ascorbic acid	13215	4.49 (475 nm)^d	36
ter-CTF-0.7	2.11	Pt	TEOA	19320	22.8 (420 nm)	31
NH_2-UiO-66/TpPa-1-COF(4:6)	2.10	Pt	Sodium ascorbate	23413	-	21
FS-COF	1.85	Pt	Ascorbic acid	10100 (±300)	3.2 (600 nm)^e	24
NTU−BDA-THTA/NH2−Ti$_3C_2$Tx(8:4)	2.09	Pt	Ascorbic acid	14228.1	9.75% (500nm)	37
FS-COF+WS5F	-	Pt	Ascorbic acid	16300 (±290)	2.2 (600 nm)^e	24
CNS-600-COF-1.3	-	Pt	TEOA	46400	31.8% (425nm)^d	38

[a]Co-1: $[Co(dmgH)_2pyCl]$; [b]Co-2: $[Co(dmgBF_2)_2(OH_2)_2]$; [c]PE: Photonic efficiency; [d]AQE: apparent quantum efficiency; [e]EQE: external quantum efficiency; [f]QE: quantum efficiency; TEOA: Triethanolamine; TEA: Triethylamine

References

1. Z. Li, Y. Zhi, P. Shao, H. Xia, G. Li, X. Feng, X. Chen, Z. Shi and X. Liu, Appl. Catal. B-Environ., 2019, 245, 334-342.
2. R. Chen, J. L. Shi, Y. Ma, G. Lin, X. Lang and C. Wang, Angew. Chem. Int. Ed., 2019, 58, 6430-6434.

3. S. Bi, C. Yang, W. Zhang, J. Xu, L. Liu, D. Wu, X. Wang, Y. Han, Q. Liang and F. Zhang, *Nat. Commun.*, 2019, **10**, 2467.
4. V. S. Vyas, F. Haase, L. Stegbauer, G. Savasci, F. Podjaski, C. Ochsenfeld and B. V. Lotsch, *Nat. Commun.*, 2015, **6**, 8508.
5. J. Thote, H. B. Aiyappa, A. Deshpande, D. Díaz Díaz, S. Kurungot and R. Banerjee, *Chem. – A Eur. J.*, 2014, **20**, 15961-15965.
6. H. Dong, X.-B. Meng, X. Zhang, H.-L. Tang, J.-W. Liu, J.-H. Wang, J.-Z. Wei, F.-M. Zhang, L.-L. Bai and X.-J. Sun, *Chem. Eng. J.*, 2020, **379**, 122342.
7. J. Ming, A. Liu, J. Zhao, P. Zhang, H. Huang, H. Lin, Z. Xu, X. Zhang, X. Wang, J. Hofkens, M. B. J. Roeffaers and J. Long, *Angew. Chem. int. ed.*, 2019, **131**, 18458-18462.
8. F. Haase, T. Banerjee, G. Savasci, C. Ochsenfeld and B. V. Lotsch, *Faraday Discuss.*, 2017, **201**, 247-264.
9. T. Banerjee, F. Haase, G. Savasci, K. Gottschling, C. Ochsenfeld and B. V. Lotsch, *J. Am. Chem. Soc.*, 2017, **139**, 16228-16234.
10. Z.-A. Lan, Y. Fang, X. Chen and X. Wang, *Chem. Commun.*, 2019, **55**, 7756-7759.
11. E. Jin, Z. Lan, Q. Jiang, K. Geng, G. Li, X. Wang and D. Jiang, *Chem*, 2019, **5**, 1632-1647.
12. L. Li, Z. Zhou, L. Li, Z. Zhuang, J. Bi, J. Chen, Y. Yu and J. Yu, *ACS Sustainable Chem. Eng.*, 2019, **7**, 18574-18581.
13. S. Bi, Z.-A. Lan, S. Paasch, W. Zhang, Y. He, C. Zhang, F. Liu, D. Wu, X. Zhuang, E. Brunner, X. Wang and F. Zhang, *Adv. Funct. Mater.*, 2017, **27**, 1703146.
14. F. Li, D. Wang, Q.-J. Xing, G. Zhou, S.-S. Liu, Y. Li, L.-L. Zheng, P. Ye and J.-P. Zou, *Appl. Catal. B: Environ.*, 2019, **243**, 621-628.
15. J.-L. Sheng, H. Dong, X.-B. Meng, H.-L. Tang, Y.-H. Yao, D.-Q. Liu, L.-L. Bai, F.-M. Zhang, J.-Z. Wei and X.-J. Sun, *ChemCatChem*, 2019, **11**, 2313-2319.
16. P. Pachfule, A. Acharjya, J. Roeser, T. Langenhahn, M. Schwarze, R. Schomäcker, A. Thomas and J. Schmidt, *J. Am. Chem. Soc.*, 2018, **140**, 1423-1427.
17. C. B. Meier, R. Clowes, E. Berardo, K. E. Jelfs, M. A. Zwijnenburg, R. S. Sprick and A. I. Cooper, *Chem. Mater.*, 2019, **31**, 8830-8838.
18. B. P. Biswal, H. A. Vignolo-González, T. Banerjee, L. Grunenberg, G. Savasci, K. Gottschling, J. Nuss, C. Ochsenfeld and B. V. Lotsch, *J. Am. Chem. Soc.*, 2019, **141**, 11082-11092.
19. S. Kuecken, A. Acharjya, L. Zhi, M. Schwarze, R. Schomäcker and A. Thomas, *Chem. Commun.*, 2017, **53**, 5854-5857.
20. W. Huang, Q. He, Y. Hu and Y. Li, *Angew. Chem.*, 2019, **131**, 8768-8772.
21. F.-M. Zhang, J.-L. Sheng, Z.-D. Yang, X.-J. Sun, H.-L. Tang, M. Lu, H. Dong, F.-C. Shen, J. Liu and Y.-Q. Lan, *Angew. Chem.*, 2018, **130**, 12282-12286.
22. L. Guo, Y. Niu, H. Xu, Q. Li, S. Razzaque, Q. Huang, S. Jin and B. Tan, *J. Mater. Chem. A*, 2018, **6**, 19775-19781.
23. N. Wang, G. Cheng, L. Guo, B. Tan and S. Jin, *Adv. Funct. Mater.*, 2019, **29**, 1904781.
24. X. Wang, L. Chen, S. Y. Chong, M. A. Little, Y. Wu, W.-H. Zhu, R. Clowes, Y. Yan, M. A. Zwijnenburg, R. S. Sprick and A. I. Cooper, *Nat. Chem.*, 2018, **10**, 1180-1189.
25. L. Stegbauer, K. Schwinghammer and B. V. Lotsch, *Chem. Sci.*, 2014, **5**, 2789-2793.
26. L. Li, W. Fang, P. Zhang, J. Bi, Y. He, J. Wang and W. Su, *J. Mater. Chem. A*, 2016, **4**, 12402-12406.
27. C. Mo, M. Yang, F. Sun, J. Jian, L. Zhong, Z. Fang, J. Feng and D. Yu, *Adv. Sci.*, 2020, **7**,

1902988.

28. K. Wang, Z. Jia, Y. Bai, X. Wang, S. E. Hodgkiss, L. Chen, S. Y. Chong, X. Wang, H. Yang, Y. Xu, F. Feng, J. W. Ward and A. I. Cooper, *J. Am. Chem. Soc.*, 2020, **142**, 11131-11138.
29. A. F. M. El-Mahdy, A. M. Elewa, S.-W. Huang, H.-H. Chou and S.-W. Kuo, *Adv. Opt. Mater.*, 2020, **n/a**, 2000641.
30. M.-Y. Gao, C.-C. Li, H.-L. Tang, X.-J. Sun, H. Dong and F.-M. Zhang, *J. Mater. Chem. A*, 2019, **7**, 20193-20200.
31. L. Guo, Y. Niu, S. Razzaque, B. Tan and S. Jin, *ACS Catal.*, 2019, **9**, 9438-9445.
32. M. Luo, Q. Yang, K. Liu, H. Cao and H. Yan, *Chem. Commun.*, 2019, **55**, 5829-5832.
33. S.-Y. Ding, P.-L. Wang, G.-L. Yin, X. Zhang and G. Lu, *Int. J. Hydrogen Energ.*, 2019, **44**, 11872-11876.
34. D. Wang, H. Zeng, X. Xiong, M.-F. Wu, M. Xia, M. Xie, J.-P. Zou and S.-L. Luo, *Sci. Bull.*, 2019, 10.015.
35. D. Wang, X. Li, L.-L. Zheng, L.-M. Qin, S. Li, P. Ye, Y. Li and J.-P. Zou, *Nanoscale*, 2018, **10**, 19509-19516.
36. Y.-J. Cheng, R. Wang, S. Wang, X.-J. Xi, L.-F. Ma and S.-Q. Zang, *Chem. Commun.*, 2018, **54**, 13563-13566.
37. H. Wang, C. Qian, J. Liu, Y. Zeng, D. Wang, W. Zhou, L. Gu, H. Wu, G. Liu and Y. Zhao, *J. Am. Chem. Soc.*, 2020, **142**, 4862-4871.
38. M. Luo, Q. Yang, W. Yang, J. Wang, F. He, K. Liu, H. Cao and H. Yan, *Small*, 2020, **16**, 2001100.